Fabrication of oxygen carrying microparticles functionalized with liver ECM-proteins to improve phenotypic three-dimensional in vitro liver assembly, function, and responses

Nic Leipzig[1], Mona Mansouri[1], Imes W.D[2], and Roberts O.S[1]

[1]University of Akron College of Engineering
[2]University of Akron Department of Chemistry

January 13, 2023

Abstract

Oxygen and extracellular matrix (ECM)-derived biopolymers play vital roles in regulating many cellular functions in both the healthy and diseased liver. This study reveals the importance of synergistically tuning the internal microenvironment to enhance oxygen availability alongside phenotypic ECM ligand presentation to promote native metabolic functions of human liver three-dimensional (3D) cell aggregates. First, fluorinated (PFC) chitosan microparticles (MPs) were generated with a microfluidic chip, then their oxygen transport properties were studied using a custom ruthenium-based oxygen sensing approach. Next, to allow for integrin engagements the surfaces of these MPs were functionalized using liver ECM proteins including fibronectin, laminin-111, laminin-511, and laminin-521. These MPs were used to assemble heterogeneous composite spheroids composed of human hepatocytes and human hepatic stellate cells. After *in vitro* culture, liver-specific functions and cell adhesion patterns were compared between groups and cells showed enhanced liver phenotypic responses in response to laminin-511 and 521 as evidenced via enhanced E-cadherin and vinculin expression as well as albumin and urea secretion. Furthermore, hepatocytes and stellate cells arranged in more phenotypic arrangements when cocultured with laminin-511 and 521 modified MPs providing clear evidence that specific ECM proteins have distinctive roles in the phenotypic regulation of liver cells in engineering 3D spheroids. This study advances efforts to create more physiologically relevant organ models allowing for well-defined conditions and phenotypic cell signaling which together improve the relevance of 3D spheroid and organoid models.

Introduction:

The need to create physiologically realistic *in vitro* liver models has resulted in the emergence of technologies such as organ on a chip, 3D printing and rotational culture methods, yielding protocols to create improved human preclinical models.[1]However, 3D cellular aggregates present certain drawbacks. First, there is no vascular network formation therefore nutrient and waste transport limits the maximum size of 3D tissues grown *in vitro.* [2] Second, *in vivo* niche-based cues such as ECM components are missing, which slows initial aggregation and cell activation resulting in loss of function and phenotype in long term cultures.[3] Unlike other organs, the liver has a unique makeup with a proportionately small ECM in relation to its volume, mainly consisting of collagen, fibronectin, and laminin.[4] Collagen represents 60% of human liver ECM molecules and constitutes mostly fibrillar collagens such as type I and III collagen,[5] providing tensile strength to the organ. Whereas non-collagenous proteins such as fibronectin and laminin are vital to maintaining basement membrane and functional integrity.[6] Fibronectin is a multifunctional adhesive glycoprotein that originally synthesized by liver cells and abundantly present in liver tissue. This protein is directly involved in regulating cellular behavior such as cell survival and proliferation.[7] Laminin is another major non-collagenous adhesive glycoprotein presents in the hepatic perisinusoidal space (space of Disse). It includes specific combinations of α, β, and γ chains giving rise to functional diversity within a common structural

framework. Within this family the distribution and expression of α5, β1 and β2 laminin chains in mammalian liver have been widely reported.[8,9]

ECM-based molecules (peptides or whole proteins) have been widely incorporated into biomaterials to promote the formation and function of various types of spheroids and organoids.[10,11]For example, human intestinal organoids were generated from pluripotent stem cells in a synthetic hydrogel based on a four-armed, maleimide-terminated poly(ethylene glycol) macromer functionalized with arginine-glycine-aspartate (RGD) adhesive peptides.[12] The authors showed that organoids encapsulated in this scaffold show high viability as well as expression levels of pluripotency, endoderm, and epithelial junction markers compared to non-modified gels. Similarly, Lin et al.[13] prepared a hydrogel based on poly (ethylene glycol)-tetra-norbornene (PEG4NB) functionalized by bioactive peptides (e.g., fibronectin-derived arginine-glycine-aspartate-serotonin (RGDS)) to improve cell–matrix interactions. They observed elevated urea secretion and Cytochrome P450 3A4 (CYP3A4) enzymatic activities, as well as upregulated mRNA levels of multiple hepatocyte genes (e.g., CYP3A4, bile salt export pump (BESP) and sodium-taurocholate cotransporting polypeptide (NTCP)) of two human hepatoma-derived cell lines (Huh7 and HepG2) encapsulated in these gels.

Despite these reports, new methodologies are needed for synthetic cellular microenvironments to reduce mass transport limitations, especially for metabolically active cell types/tissues such as the liver. Various methodologies have been formulated to promote oxygen transport and maintain viability as well as the function of cells in 3D culture.[14,15] In our recent work, we created PFC-MPs to overcome common limitations of spheroids such as inadequate oxygen supply and ultimate loss of cell/organ specific functions over long-term cultures.[16] Our data suggested that PFC- conjugated MPs offer a simple, affordable, and direct approach for improving mass transport of nutrients within spheroids and other engineered tissues. In the present study, we extended our PFC-MP approach to yield improved hepatic 3D cell culture models using ECM components. First, we examined if PFC- MPs play a role in driving oxygen into spheroidal aggregates using optical sensing. Then, we covalently tethered ECM proteins including laminin-111, laminin-511, laminin-521, and fibronectin on the surface of PFC- MPs followed by co-culturing these particles with two immortalized human liver cells including human hepatoma (HepG2) and hepatic stellate cells (HSCs). We characterized liver-specific synthetic functions and cell adhesion patterns, which allowed us to collect evidence that different ECM proteins presented from PFC-MPs have distinctive roles in the physiological regulation of liver cells *in vitro* 3D culture.

Experimental Section

Microparticle synthesis and characterization

PFC-MPs were synthesized using a T-shaped polydimethylsiloxane (PDMS) droplet generator as previously described.[16]Briefly, using oil (span80, Sigma Aldrich, cat# 1338-43-8) as a continuous phase in the two side channels and polymer solution as the dispersed phase in the middle channel, we produced a steady stream of homogenous PFC- MPs. These MPs were passed through a glass tube and polymerized using the photoinitiator Lithium phenyl-2,4,6-trimethylbenzoylphosphinate (LAP,0.1wt% in distilled water, Sigma-Aldrich, cat# 85073-19-4) included in the polymer phase, under the irradiation of a lamp (600-700 nm). The composition of MPs was characterized via X-ray photoelectron spectroscopy (XPS) with a scanning monochromated Al Kα (117.40 eV; 25.0 W; spot size, 100 μm). The take-off angle between the sample surface and analyzer was 45.0°, and the X-ray beam collected C1s, N1s, F1s, and O1s elemental information. We also tested the MPs using thermogravimetric analysis (TGA) to study their thermal stability. 5 mg of PFC- MPs were weighed and placed in an open pan (platinum 100 μL) attached to a microbalance (TGA550, TA Instruments). The sample was heated at 10 °C.min^{-1} from 25 to 700 °C under dry nitrogen in standard mode with a ramp test type.

Studying oxygen levels in MPs

We used the ruthenium complex Tris(4,7-diphenyl-1,10-phenanthroline) ruthenium (II) dichloride (Santa Cruz, cat#sc-216023B), or RuDPP, as an oxygen sensing molecule. RuDPP shows a large Stokes shift by emitting orange light (610 nm peak) when excited with blue light (455 nm peak). We used a custom-made

chamber with two inlets for sample and gas**(Figure S1)** , a CCD camera (Hamamatsu ORCA-R2/model: C10600-10B), and HCImage Live software (version 4.8.3.0, Hamamatsu Corporation, NJ) to measure light intensity. 1 mg of RuDPP was dispersed in 1X phosphate buffered saline (PBS) solution (pH=7.4) with or without PFC-MPs (10 $mg.ml^{-1}$) and sonicated thoroughly before getting injected into the channel. A light emitting diode (LED, $4\mu W.cm^{-2}$) was used as the excitation source (peak wavelength 455nm) and a long wave pass filter (Thorlabs, FMP1, cutoff wavelength 600 nm) was used to minimize unwanted wavelengths. We compared the oxygen level within the chamber using two gases including nitrogen (N_2) and oxygen (O_2) to represent 0% and 100% oxygen, respectively. N_2 gas was initially injected into the channel followed by imaging and then the gas source was switched to O_2 to present a saturated state. For each condition, 8 frames per second were obtained for up to 60s. The fluorescent intensity of unquenched images (I_0) was divided by quenched images (I) on a frame-by-frame basis to obtain a Stern-Volmer image.

Preparation of liver spheroids incorporated with PFC- MPs

Creation of spheroids and incorporation with MP followed procedures recently published.[16] Briefly, HepG2 and HSC cells were used for *in vitro* experimentation. Low glucose Dulbecco's Modified Eagle's Medium with L-glutamine and sodium bicarbonate (DMEM; Sigma Aldrich, cat#D6046) supplemented with fetal bovine serum (10%v/v, FBS, R&D systems, cat# S11150) and penicillin/streptomycin (1%v/v, P/S, Thermofisher, cat# 15070-063) was used for expansion of HepG2 cells. For HSC cells, High glucose DMEM containing L-glutamine, sodium pyruvate, sodium bicarbonate (Sigma Aldrich, cat#D6029), 10% v/v FBS and 1% v/v P/S was used. The fabrication of cell spheroids with MPs utilized previous findings.[16] Briefly, HepG2 and HSC cells were mixed at a 4:1 ratio, then added to MPs to achieve a desired final cell to particle ratio (150:1) and transferred to the 96-well cell repellant plates (CELLSTAR® Plates with Cell-Repellent Surface, cat#: 650970) at a seeding density of 20,000 cells/well. Cells were overlaid with a serum-free and defined hepatocyte culture media (Corning®, cat# 355056). To form cell aggregates, the well plate was centrifuged at 300 × g for 5 min.

Measurement of oxygen concentration within spheroids

For oxygen characterization, RuDPP was added to cell suspensions (2 $\mu g.ml^{-1}$) before spheroid formation. After 5 days of culture the spheroids were live imaged using a laser scanning confocal microscope (Olympus FV1000) to capture Z-stack images throughout the spheroids. μ-Slide 8 well glass bottom slides from ibidi (cat# 80827) were used to image spheroids (excitation: 455nm, emission: 610nm). The imaging was performed by taking z-stacks at 10 μm intervals using 4X magnification. The fluorescent signals for spheroids cultured with/without PFC-MPs were quantitatively and spatially assessed using ImageJ (National Institutes of Health, Bethesda, MD, USA). To correlate fluorescent intensity to concentration of oxygen, a calibration curve was generated for RuDPP relating fluorescent intensity versus various oxygen concentrations ($\%O_2$).

Surface functionalization of MPs using liver adhesive ligand

The protocol for covalent bonding of proteins on PFC- MPs was similar to that reported in previous studies.[17] The activation of proteins was achieved by mixing 10 $\mu g.ml^{-1}$ of each respective ECM protein solution for 30 minutes at room temperature in a solution containing 2mM*N* -ethyl-N'-(3-dimethylaminopropyl) carbodiimide (EDC) (Sigma Aldrich, cat# E7750) in ultrapure water (18.2 MΩ) and 5mM N-hydroxysuccinimide esters (NHS) (Sigma Aldrich, cat#130672) in 0.1M 2-(N-morpholino) ethanesulfonic acid hemisodium salt (MES) buffer (Sigma Aldrich, cat#M3671. PFC- MPs were also dispersed in 0.1M MES and their pH was adjusted to four different values including 5.90, 6.20, 6.50, and 6.80 by addition of 1M NaOH. Afterward, activated proteins were added to the particles to react with the free amino groups available on MP surfaces. The mixture was kept under mild shaking for 5 h at room temperature, dialyzed for 48h using SnakeSkin Dialysis Tubing (3.5K MWCO, Fisher scientific, cat#PI68035) against distilled water included 0.05% triton 100X (Sigma Aldrich, cat#X100-100ML) and then freeze-dried. The amount of protein conjugated to MPs was measured by Bicinchoninic acid (BCA) assay (Thermofisher, cat# PI23235) using manufacturer's directions, as well as via XPS surface analysis, as described above. For simplicity, we picked MPs decorated with laminin-111 as a model to study efficiency of protein grafting.

Functional characterization of liver spheroids

After spheroids were cultured with functionalized MPs, levels of albumin were determined using a commercially available kit (QuantiChrom BCP Albumin, BioAssay Systems, cat# DIAP-250) as a measure of liver cells' function. The experiment was performed according to the manufacturer's instructions. Briefly, the medium was collected on days 5 and 10. A 20 µl aliquot was used to measure albumin secretion into the medium. 200 µL of working reagent was added and after 5 min incubation at room temperature, the optical density at 590-630 nm (peak absorbance at 610 nm) was read by a plate reader (Tecan Infinite M200, Tecan Austria GmbH, Austria). Urea was also measured by the QuantiChrom Urea Assay Kit (BioAssay Systems, cat# DIUR-100,) using a similar procedure to the albumin kit. 5 µL of sample was mixed with 200 µL of working reagent, incubated for 20 min, and absorbance was read at 520 nm by plate reader.

Histologic and immunohistochemical examinations

For immunofluorescence staining of 3D liver spheroids, spheroids were fixed for 30 min in 4% w/v paraformaldehyde in PBS. Then whole samples were permeabilized with 0.1% v/v Triton X-100 in PBS for 5 min and pre-blocked for 30 min with 10% FBS diluted in PBS. Next, spheroids were incubated with mouse glial fibrillary acidic protein (GFAP; 1:50, Developmental Studies Hybridoma Bank (DSHB), cat # 8-1E7) for HSCs, rabbit CYP3A4 antibody (1:200, Fisher Scientific, cat# 50-173-2058) for HepG2 cells, anti-human E-cadherin monoclonal antibody (1:200, R&D, cat# MAB1838) and anti-vinculin antibody (1:200, Santa Cruz, cat# sc-25336) overnight in the fridge. The next day we stained the spheroids with Alexa Fluor 546 goat anti-mouse IgG (H+L) highly cross-adsorbed secondary antibody (Thermofisher, cat# A11030) and Alexa Fluor 546 donkey anti Sheep IgG (H+L) Secondary Antibody (Thermofisher, cat # A21098) for 90 min, as appropriate. The spheroids were then incubated with 10 µM Hoechst 33342 (Thermofisher, cat# H3570) diluted in 1% BSA for nuclei detection for 5 min before collecting confocal microscope images (Nikon Corporation confocal microscope, inverted). The step size of Z-stacks was set to 10 µm thickness and 30-40 slices per image were taken to image entire spheroids.

Data analysis

Data processing and displaying were performed using GraphPad Prism 5 (GraphPad Software, USA). Mean and standard deviation were displayed for all data sets. Statistical significance was determined using either Student's t -test or two-way ANOVA followed by Tukey's *post hoc* test ($p < 0.05$). Groups with significant differences are shown with alphabetic letters to signify ranking of means. Groups indicated with the same letters were not found to be significantly different.

Results and Discussion:

Characterization of PFC- MPs

It has been well established that oxygen carrying properties of PFC-MPs stem from the PFC substitutions, [18,19] therefore in this report we focused on studying the composition of microfluidic generated MPs while confirming the presence of PFC molecules**(Figure 1). Figure 1B** shows the TGA spectrum of crosslinked non-PFC-MPs and PFC-MPs. The weight loss in both spectra begins at approximately 90°C and continues until 130°C which is likely associated with loss of absorbed water in the crosslinked MPs. Based on these data both MPs were able to absorb water correlating to ˜25% via hydrophilic moieties in chitosan.[20] Another major mass loss stage is observed between 280-400°C, which is related to thermal decomposition of chitosan.[21] Overall, around 43.1% w/w of PFC-MPs and 52.82% w/w of non-PFC-MPs were lost when heated above 400°C, suggesting higher thermal stability of PFC-MPs compared to non-PFC-MPs. Carbon–fluorine (C-F) bonds in PFC molecules are strongly polarized, which accounts for their thermal stability.[22] Next, XPS was used to provide a quantitative analysis from the outer 10 nm of MP surfaces. XPS spectra showed carbon (C1s at 284.7 eV) and oxygen (O1s at 531.5 eV) as well as fluorine (F1s at 688.6 eV) on surface of PFC-MPs **(Figure 1C),**suggesting the presence of PFC molecules on the surface of MPs. This is expected since the particles were crosslinked while still in the oil phase. We tried Fourier-transform infrared spectroscopy (FTIR) as well**(Figure S2)** ; however, due to PFC abundance being lower than the detection

threshold (2 wt%), we could not detect C-F bonds.

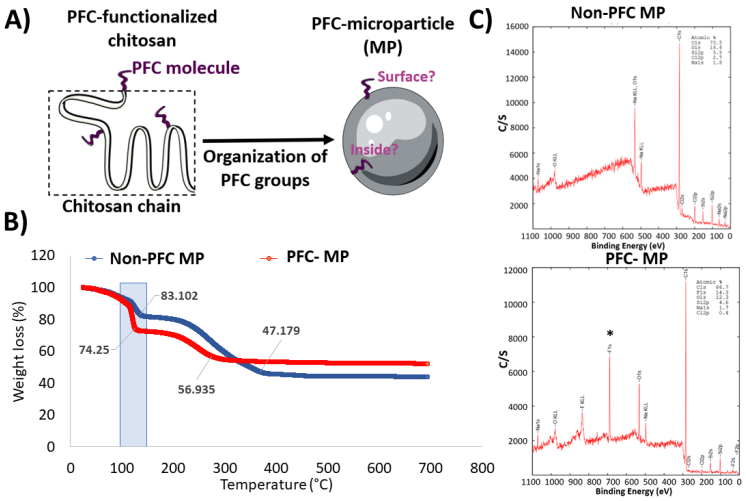

Figure 1: A) Studying the arrangement of PFC molecules after MP formulation B) Thermal degradation study of MPs using TGA to assess their stability. The shaded box shows temperature rand of interest (100-150°C). C) Characterization of PFC modified and non-PFC modified MPs using XPS. The resulting spectrums showed a sharp peak related to PFCs, suggesting availability of PFC groups on the surface. * refers to fluorine spectrum located at 688.6 eV.

Assessing oxygen carrying properties of MPs using RuDPP

In our previous studies, PFC conjugated chitosan hydrogels were tested for oxygen transport properties using commercial phosphorescent dots[23] and needle sensors.[24]Our investigations showed these hydrogels enhanced oxygen transport in aqueous conditions and allowed oxygen tensions to reach higher equilibrium states compared to controls not integrating PFCs. In this study, we were interested in understanding the impact of our PFC-MPs on oxygen tensions using RuDPP in finer detail and at a cellular level. RuDPP has a long fluorescence lifetime and a long Stokes-shift. It quenches in the presence of oxygen and thus is a suitable probe dye for determining dissolved oxygen.[25] A mixture of MP solution and RuDPP in PBS was injected into a sealed, custom-built chamber and exposed to gases (**Figure 2A)** . We measured the fluorescence intensity after flowing pure N_2 and pure O_2 gasses to create oxygen partial pressures at the extremes of 0% oxygen and 100% oxygen in solution. A solution without any MPs was used as a control. As shown in **Figure 2B** , when switching from pure N_2 to pure O_2, the fluorescent intensity decreased due to oxygen quenching of RuDPP. We also observed a decrease in fluorescence intensity in the presence of MPs which can be attributed to increased dissolved oxygen concentration. The sensitivity of the optical oxygen sensor with (I) and without (I_0) a quencher (here oxygen) was quantified in term of the ratio I_0/I_{100}, as shown in **Figure 2C** at equilibrium. Our results indicated that the solution containing PFC-MPs exhibited the highest sensitivity to oxygen with the maximum quenching ratio ofI_0/I_{100} =1.1. Following saturation, we then stopped oxygen flow and studied the release kinetics. We observed that the control group showed complete RUDPP recovery within 3 min whereas MPs slowed the RuDPP recovery process to 10 min **(Figure 2D)** . This can be explained by MPs' ability to uptake oxygen and then release it gradually into a low oxygen tension aqueous environment. These results confirm that PFC-MPs can act as both an oxygen absorbing material as well as a reservoir to release oxygen gradually in an aqueous environment. This finding is in agreement with our earlier work with PFC-modified hydrogels where we examined their ability to deliver and sustain biological levels oxygen for enhancing cellular functions essential in wound healing.[26,27] Most recent evidence from another research group shows the potential of PFC nanoemulsions as artificial oxygen carriers.[28] In this study, PFC nanoemulsions exhibited five times higher dissolved O_2 concentration

compared to water, as measured by a submerged O_2 probe.

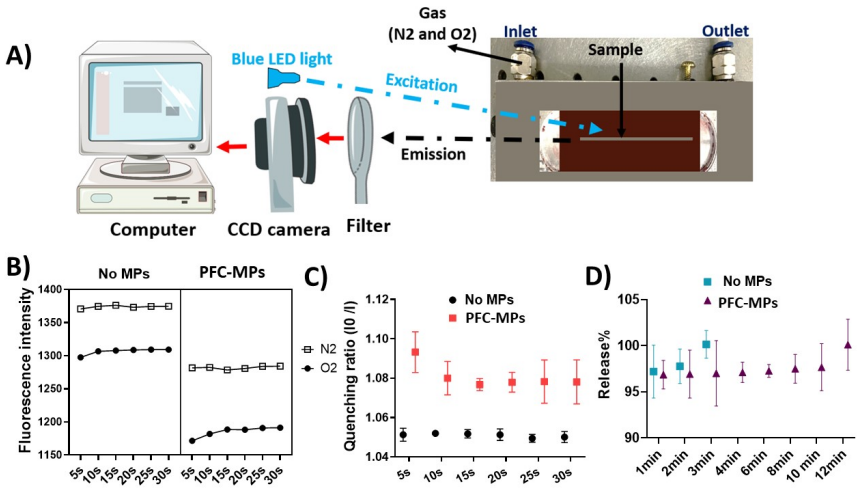

Figure 2: A) Illustration of custom-built oxygen sensing measurement setup with CCD camera, excitation light, selective filter, and flow chamber. B) Fluorescence emission spectra at different oxygen (0% and 100%) concentrations excited at 455nm measured by CCD camera equipped with a telecentric lens. C) Relative fluorescent intensity of Stern-Volmer equation over time obtained by dividing values of unquenched and quenched fluorescence intensities (I_0/I) representing the oxygen concentration in the chamber. D) MPs oxygen release kinetics containing following saturation with 100% oxygen. The intensity of each condition was obtained by averaging the intensity over the channel.

Oxygen levels within live spheroids cultured with/without PFC-MPs

To better understand MP effects on oxygen levels in our spheroid model, we used RuDPP and fluorescent microscopy building upon our earlier validation experiments without cells. For the spheroid system, we mixed cell suspension with different amounts of RuDPP to find an optimum concentration required for the formation of spheroids with RuDPP**(Figure S1A).** Although the working concentration of dye in our system is low, we were able to utilize this concentration to directly image intracellular oxygen levels. To study cellular oxygen levels throughout spheroids we made 3D images of z-stacks and looked at the fluorescence intensity throughout the whole spheroid as shown in**Figure 3A** . We observed cells at higher oxygen tensions (shown in black) in spheroids cultured with PFC-MPs, demonstrating that MPs improve oxygen levels in the spheroids. Quantitative cellular measurements corresponding O_2% were performed via a calibration curve based on RuDPP in a controlled oxygenated environment**(Figure S1C).** To perform this, we focused on individual cells and the intensity of those cells along a line drawn in a central confocal plane of spheroids. As shown in **Figure 3B,** the addition of MPs increased oxygen levels from 7 to 10%, emphasizing the validity of our approach. In related work, partial pressure of oxygen (PO_2) levels in human colorectal spheroids with a diameter of 600 μm were measured using electron spin resonance (ESR) microscopy, and PO_2 values were reported in the range of 50-60 mmHg which is equivalent to 6.6-7.9% oxygen at inner regions.[29] *In vitro* experiments are usually performed in incubators that maintain a PO_2 of ˜142 mmHg (18.7% oxygen), whereas cells in our body do not experience a PO_2 greater than 100 mmHg (13% oxygen). Despite lower oxygen tensions *in vivo* , cells can tolerate these levels and easily survive because of short transport distances from supply via blood vessels.[30] When it comes to avascular 3D cell aggregates, especially larger ones, we expect lower PO_2 due to greater distances and mass transport limitations. The Hypoxyprobe (pimonidazole hydrochloride) method is often used to study hypoxia responses in spheroids;[31] however, the method is an indirect endpoint test with no quantitative analysis in terms of oxygen tensions. Using RuDPP is advantageous for live and kinetic imaging since the fluorescence lifetime of RuDPP is largely insensitive

to pH, ion concentrations, and cellular contents, making it suitable for cell culture applications.[32] Previous work has shown that MCF-7 cells labeled with RuDPP at a concentration of 20 μg.mL^{-1} maintained 90% viability after 24h,[33] confirming its biocompatibility.

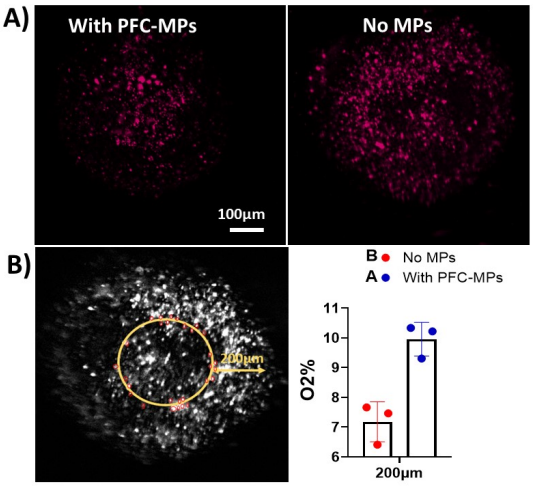

Figure 3: Visualizing oxygen within liver spheroids using RuDPP as an oxygen sensing dye, which quenches fluorescence emission in the presence of sufficient oxygen. A) Reconstruction of a 3D spheroid and intensity variance throughout the spheroid cultured for 5 days. PFC- MPs resulted in lower fluorescence intensity compared to the control which did not have any MPs. B) Measurement of intensity of individual cells along a circular line in a central plane of spheroids with quantitative data. The average intensity of bright dots around each line was quantified and converted to O_2% via a calibration curve. Data represented as mean ± SD. n = 3 independent spheroids, one-way ANOVA and Tukey's *post hoc* .

Covalent immobilization of liver ECM adhesive ligands to PFC-MPs

Next, we modified MP surfaces by covalently binding ECM proteins to overcome the limitations associated with simple physical adsorption of ECM proteins, including their undesired conformational changes and release from surfaces over time.[34] In this study, biofunctionalization with the ECM proteins plasma fibronectin, laminin-111, 511, and 521 to the surface of PFC-MPs was accomplished by a coupling reaction between the carboxyl residues of proteins to the free amine residues of chitosan using EDC as crosslinker and NHS ester as an enhancer of coupling **(Figure. 4A)** . The EDC/NHS coupling reaction is a selective method for preservation of biological activity of the protein and has previously been applied in the production of protein functionalized chitosan derivatives.[35–37] Since the pH of the reaction solution is critical for maximizing the amination reaction, we tested different pH levels keeping all other conditions the same, to determine the favored pH to maximize attachment. The recommended pH conditions for the carbodiimide reaction via EDC/NHS is in the range of pH 4.5–5.5.[38] However, due to the presence of amine groups, chitosan based materials become protonated at a pH below pK_a 6.0.[39] Between a pH of 5.9 and 6.8 we achieved ligand conjugation on MPs ranging from 2 to 3.5 μg.ml^{-1}, as quantified by BCA kit **(Figure 4B)** . We can attribute the poorer yield at the lowest pH (5.9) to high chitosan protonation, resulting in a slower reaction. Poor yield at the highest pH (6.8) might be due to the formation of macroscopic aggregates resulting in reduced availability of surface area for reactions. The formation of aggregates at pH >6.5 where chitosan particles are weakly charged and less stable was reported previously.[40,41] We further characterized the uncoated and coated MPs modified at different pH levels via XPS.**Figure 4C** presents atomic compositions of MPs modified at different pHs. This result shows an increase in atomic nitrogen percentages (N1s%) as a reliable marker to detect additional amide groups (N–C=O) from amino acids in added ECM proteins compared to non-modified MPs. Interestingly, we observed an increase from 0.9% to 6.0% at pH=6.2 which

confirms the data obtained from colorimetric quantification. Similarly, Huang and coworkers evaluated the grafting efficiency of laminin (derived from Engelbreth-Holm-Swarm mouse sarcoma basement membrane) on poly(lactic-co-glycolic acid) (PLGA) film using XPS and observed an increase in N1s from 0.5 to 1.1% after modification with laminin.[42] We opted to focus on only N1s because C1s and O1s peaks can originate from the MP composition itself and might lead to misleading data.

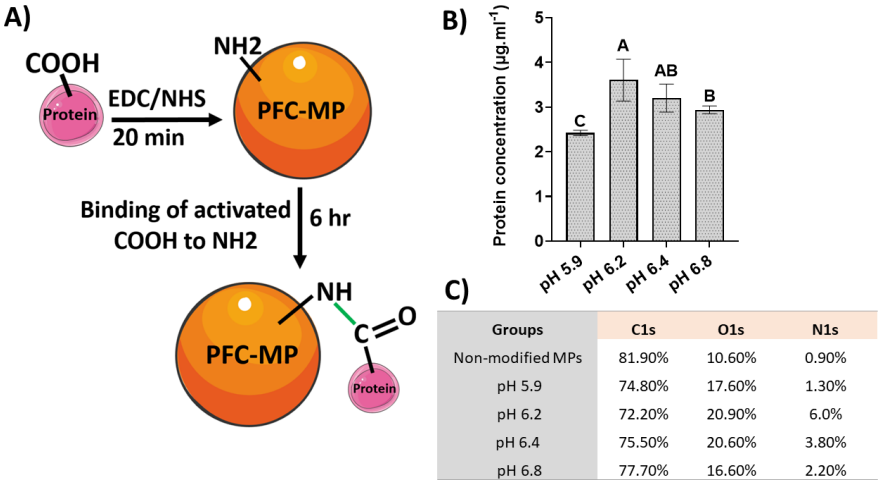

C)

Groups	C1s	O1s	N1s
Non-modified MPs	81.90%	10.60%	0.90%
pH 5.9	74.80%	17.60%	1.30%
pH 6.2	72.20%	20.90%	6.0%
pH 6.4	75.50%	20.60%	3.80%
pH 6.8	77.70%	16.60%	2.20%

Figure 4: EDC/NHS coupling reaction for bioconjugation of ECM proteins to MPs. A) Schematic of EDC/NHS reaction between protein carboxyl residues and free amine groups from PFC- oxygenating MPs in varied pHs. B) Quantification of covalently tethered protein (laminin 111) via BCA assay kit. Data represented as mean ± SD, n = 4. Statistical analysis via one-way ANOVA with Tukey's *post hoc*testing with A as the highest mean and C with the lowest mean. C) Atomic composition of modified and non-modified PFC- MPs measured via XPS. The N1S percentage correlates to the concentration of proteins attached to the surface.

Influence of specific ECM proteins on liver-specific functions

After confirming successful covalent ECM tethering to MPS, we moved to assess biological responses in spheroids by combining hepatocytes and stellate cells with modified MPs **(Figure 5A)** , specifically to study potential impact of different ECM proteins on liver-specific functions. In culture, viable hepatocytes synthesize and excrete albumin and urea into the surrounding medium, replicating important functions they perform *in vivo* in the liver. To characterize these critical cellular functions, we collected culture medium and measured albumin and urea production at specific time points.

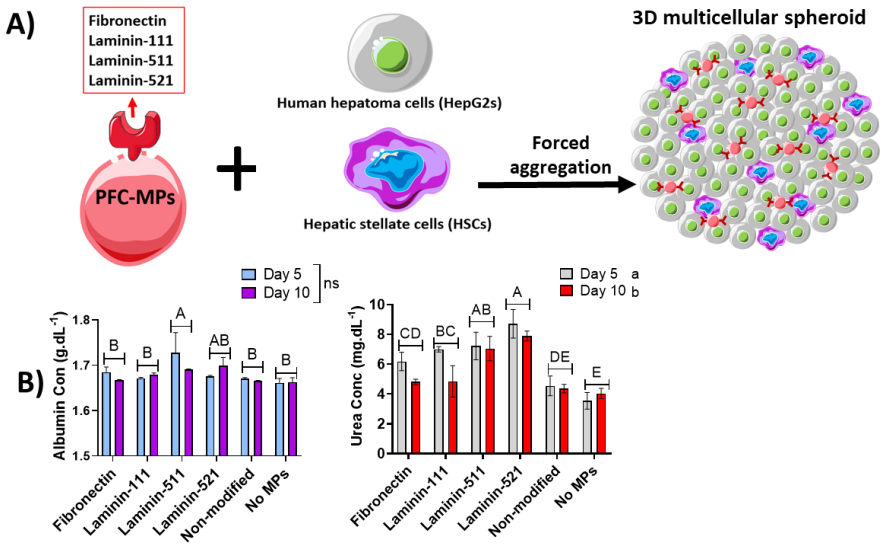

Figure 5: Schematic of experimental procedure for formation of enhanced spheroids using ECM modified oxygenating MPs and two liver cell lines. B) Quantification of albumin and urea secretion into the media over the culture period (10 days). Data represented as mean ± SD. n = 3 independent spheroids. Statistics via two-way ANOVA followed by a Tukey's *post hoc* testing.

As **Figure 5B** shows, the more mature laminin isoforms 511 and 521 boosted albumin and urea production compared to the other groups ($p < 0.01$), providing evidence that these two isoforms can more closely reflect the *in vivo* composition of cells present in the liver. Consistent with this interpretation laminin-511 and -521 coated surfaces were proved to improve culture matrices for hepatic specification and differentiation of human pluripotent stem cells (hPSCs),[43] as well as human embryonic stem cells (hESC).[44] We also considered laminin-111 to represent a variation of laminin not found abundantly in the adult liver to compare the difference between liver specific isotypes to non-specific ones. Laminin-111 is expressed during embryogenesis and plays an important role in assembling early basement membranes.[45] We did not find any significant differences ($p > 0.05$) between laminin-111 conjugated and non-coated MPs in terms of liver specific functions probed, highlighting the importance of proteins native to the mature *in vivo* liver environment for benefitting cell culture *in vitro* . Our result is consistent with an experiment conducted by Klaas et. al[46] where they cultured HepG2 cells on 3D nano- and microfiber structures based on gelatin, preincubated with laminin-111 and observed no significant changes in cell morphology, viability and production of proteins between coated with laminin-111 and uncoated 3D gelatin scaffolds.

Visualizing cell-cell and cell-ECM interactions

Improved function in response to laminin modified MPs, further strengthened our hypothesis that effects exerted on cells by various ECM ligands can be differently sensed and translated by cells. To investigate ECM activation events, we used immunofluorescence staining to probe for vinculin and cadherin expression in spheroids. Vinculin is a common component of activated focal adhesion complex when cells are actively engaging ECM with integrin receptors. Cadherins are essential constituents of adherens junctions, important in the formation and maintenance of cell-cell contacts.[47]

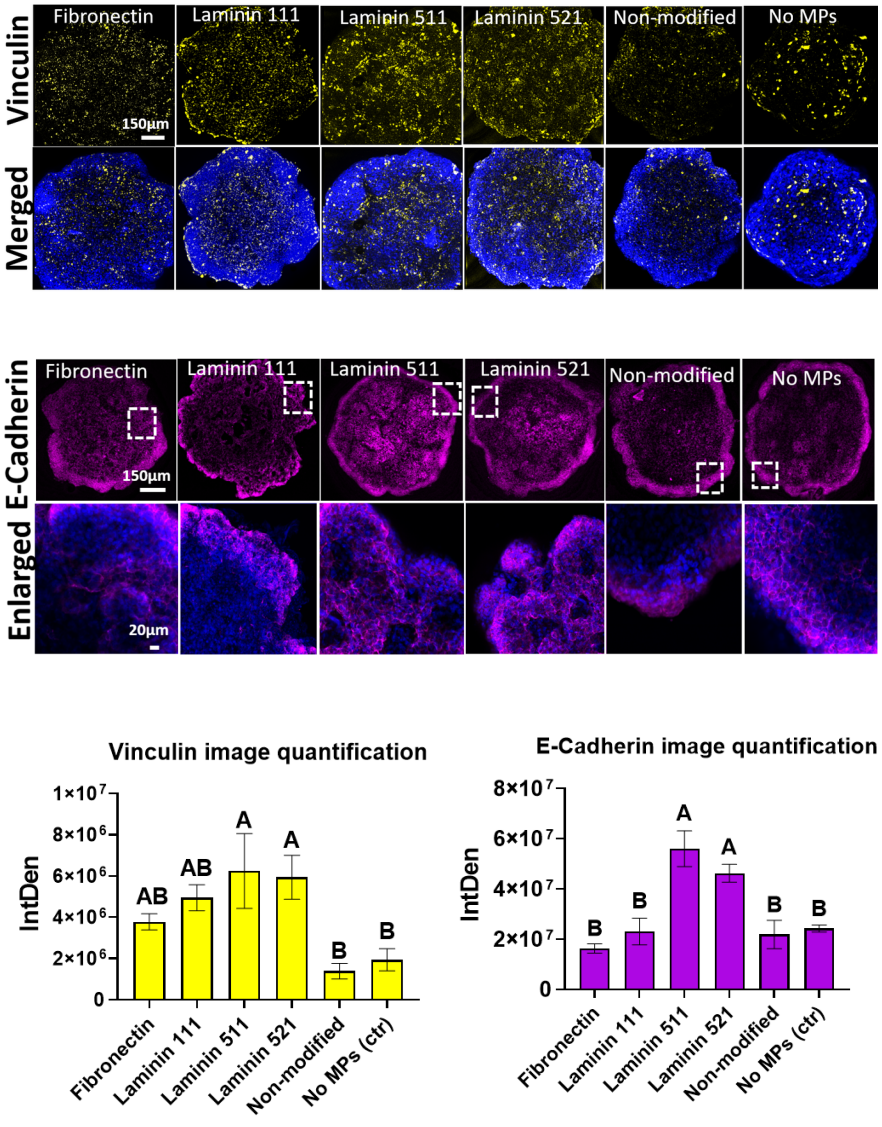

Figure 6: Immunofluorescent staining of fixed spheroids composed of HepG2s:HSCs (4:1), 20k cells initially per spheroid cultured with different oxygenating MPs for 10 d stained with A) Anti-Vinculin (for focal adhesions, yellow), B) E-Cadherin (for adherens, purple), and Hoechst 33342 (for nuclei, blue) using confocal microscopy on central plane. C) Quantitative analysis of images using ImageJ. Statistics via one-way ANOVA and Tukey's *post hoc* testing with A as the highest mean and D with the lowest mean, $p < 0.05$. Mean ± SD, n =2 spheroids with S=3.

Figure 6A shows representative confocal microscope images of liver spheroids cultured with various modified MPs and stained for vinculin. We observed high levels of vinculin expression in the laminin-511 group suggesting better integrin mediated focal adhesion kinase (FAK) activation and focal adhesion formation. In connection to our findings, the Mitaka group investigated the deposition of laminins containing the α5 chain in the liver cancer environment and concluded that laminin-511 and -521 are major isoforms in liver tumors. They showed that cancer cells could specifically interact with these ligands through integrin α3β1 and α6β4 which are widely expressed in hepatocellular carcinoma.[48,49] Laminin-111 primary binding integrins are α6β1[50] and α7β1[49] while fibronectins main integrin receptors are α5β1, α8β1, αVβ1.[51] HepG2 cells are

known to express α2, α6, β1, and β4 integrin subunits[52] and very low levels of the fibronectin receptors, presenting the possibility that they may respond to laminin-511 and 521 but not fibronectin and laminin-111 simply because they do not express the appropriate integrin receptors.

Equally important in the liver to integrin activation is cell-cell adherins formation. Hepatocytes in the liver arrange with one surface in direct contact with blood and the other surface forming tight junctions with adjacent cells. For every eight hepatocytes, one HSC helps to maintain the storage of vitamin A and protects hepatocytes in case of injury.[53] Thus, we studied physical linkage between cells to explore the effect of modified MPs on E-cadherin expression levels. E-cadherin, a cell-cell adhesion molecule in epithelial tissues, is localized on the surfaces of cells and allows physical linkage between neighboring cells. [54]**Figure 6B** shows increased expression of E-cadherin in spheroids cultured with laminin-511 and -521 modified MPs as compared with other groups ($p < 0.01$). Importantly, we observed high expression of E-cadherin at the edges, which is associated with more heterotypic cell-cell contacts. The degree of E-cadherin contact has been shown to affect proliferation and liver-specific function.[55] Taken together, analysis of vinculin and E-cadherin expression suggest that the phenotype of cells was maintained better in groups cultured with laminin-511 and -521 and may indeed play a role in modulating hepatocytes functions. Another important aspect of adherens-type junctions is stabilization of the interactions between adjacent cells, which is a crucial factor in forming and maintaining 3D cellular aggregates. In our previous study with liver spheroids,[16] we showed that HSCs play a central role in compactness and formation of stable liver spheroids. Improved E-cadherin expression prompted us to determine if we could use MPs modified with laminin 511 or 521 instead of HSCs to induce the cells form compact spheroids. Our data suggested that although these MPs lead to smaller size spheroids and more cell-cell junctions compared to HepG2 only spheroids **(Figure S3),** they failed to achieve the compactness caused by HSCs. This is likely because HSC secrete many biomolecules, cytokines, and growth factors leading to better shape and stability. In the liver, HSCs do not constitute direct cell adhesions with liver sinusoidal endothelial cells (LSECs), whereas they establish adherens junctions with hepatocytes through thorn-like microprojections or spines [56] with E-cadherin as the main adhesion molecule.

Visualizing cell arrangements

In vivo , ECM molecules including fibronectins, collagens, and laminins not only affect signaling properties and cell function but also modulate overall tissue architecture with direct consequences on cell arrangements and tissue organization.[57] To better understand the effects of specific ECM proteins on the cell organization, we used immunohistochemistry staining for HepG2 and HSC cells in whole mount spheroids to visualize the impact of ECM modified MPs on arrangements **(Figure 7)** . Although HepG2 cell distribution was homogenous, we observed distinct localization of HSCs toward the periphery of spheroids, generating a distinct outer layer of similar thickness in all groups. This also correlates with E-cadherin staining results (**Figure 6B**). The contacting area of the hepatocytes contains collagen fibrils, [58]resulting in a membrane thickening which we also observed in our images (the purple ring at the edge of all groups). We observed that groups treated with laminin-511 and 521 resulted in localization of some HSCs toward the center of spheroids, perhaps because PFC-laminin 511/521 MPs stimulate cells to change position relative to their neighbors toward contact strengthening. This finding lends support to prior findings and confirms that interactions between cells and the ECM at integrin-based adhesion sites allow cells to sense their physical surroundings and adjust mechanisms of migration and anchorage.[59]Thus, besides organization, our co culture system provides a similar physicochemical structure that more closely mimics *in vivo* tissue counterparts.

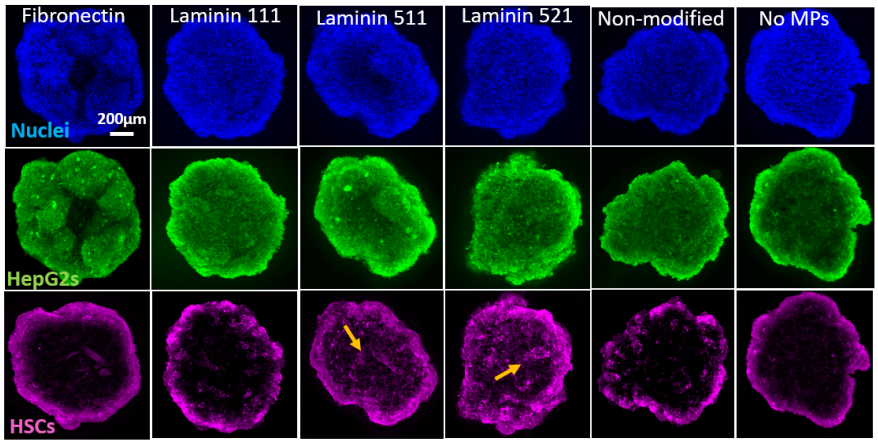

Figure 7: Cell heterogeneity in spheroids using HepG2: HSC (4:1), 20k cells initially per spheroid cultured with different oxygenating MPs. A) Representative confocal microscopic images of central plane of spheroids stained with CYP3A4 (for HepG2 cells, green), GFAP (for HSC cells, purple), and Hoechst 33342 (for nuclei, blue). Arrows highlight the localization of HSCs. B) Quantitative analysis of images using ImageJ. Statistics via one-way ANOVA and Tukey's *post hoc* testing with A as the highest mean and C with the lowest mean, $p < 0.05$. Mean ± SD, n =2 with S=3.

Conclusions

In this study, we demonstrated a new strategy for improving cellular assembly and functions inside human cell-based spheroids via synergistically promoting biophysical and biochemical cues using engineered MPs. Our MPs integrated covalently attached PFC groups and ECM adhesive ligands on the surface to enhance oxygen tensions internally while improving cell/tissue architecture and functions, respectively. We confirmed the value of PFC-MPs for dissolving and releasing oxygen to enhance oxygen tensions at the cellular level using a RuDPP oxygen sensitive dye with microscopy-based fluorescence sensing. We next observed that cells in assembled liver spheroids responded best to MPs presenting laminin-511 and -521 ECM proteins, which are more prevalent in the mature liver as compared to laminin-111. These laminin isoforms encouraged enhanced phenotypic liver spheroid formation with up-regulation of E-cadherin and vinculin expression, as well as greater albumin and urea secretion as compared to MPs presenting other ECMs and the controls. HSCs also arranged in native liver type arrangements when laminin 511/521 conjugated MPs were used as compared to laminin-111, fibronectin, and control groups; providing evidence that ECM proteins have distinct roles in the phenotypic regulation of mature liver derived cells. In conclusion, via synergistic enhancement of internal oxygen availability as well as presentation of specific ECM cell adhesion ligands, our engineered MP approach provides a unique tool to help cells to assemble in a more native 3D microenvironment within spheroids, thereby improving *in vitro* modeling applications such as in the first stages of drug development or for personalized drug screening applications.

Acknowledgments

We would like to acknowledge partial funding from the University of Akron. We are also grateful to Dr. Ali Dhinojwala for his valuable suggestions and discussions regarding MP characterization and Chinnapatch Tantisuwanno for technical assistance in conducting Thermogravimetric testing and analysis.

References

[1] A. Khanna, M. Zamani, N. F. Huang, *J. Cardiovasc. Dev. Dis. 2021, Vol. 8, Page 137* **2021** , *8* , 137.

[2] M. Mansouri, N. D. Leipzig, *Biophys. Rev.* **2021** ,*2* , 021305.

[3] S. Nagata, F. Ozawa, M. Nie, S. Takeuchi, *PLoS One***2020** , *15* , e0234441.

[4] A. Martinez-Hernandez, P. S. Amenta, *Virchows Arch. A 1993 4232* **1993** , *423* , 77.

[5] H. Nyström, *Semin. Cancer Biol.* **2021** , *71* , 134.

[6] E. Arriazu, M. R. De Galarreta, F. J. Cubero, M. Varela-Rey, M. P. P. De Obanos, T. M. Leung, A. Lopategi, A. Benedicto, I. Abraham-Enachescu, N. Nieto, *Antioxidants Redox Signal.***2014** , *21* , 1078.

[7] R. S. Aziz-Seible, C. A. Casey, *World J. Gastroenterol.***2011** , *17* , 2482.

[8] Y. R. Lou, A. W. Leung, *Biotechnol. Adv.* **2018** ,*36* , 132.

[9] Y. Kikkawa, Y. Mochizuki, J. H. Miner, T. Mitaka, *Exp. Cell Res.* **2005** , *305* , 99.

[10] T. Saydé, O. El Hamoui, B. Alies, K. Gaudin, G. Lespes, S. Battu, *Nanomaterials* **2021** , *11* , 1.

[11] M. W. Tibbitt, K. S. Anseth, *Biotechnol. Bioeng.***2009** , *103* , 655.

[12] R. Cruz-Acuña, M. Quirós, A. E. Farkas, P. H. Dedhia, S. Huang, D. Siuda, V. García-Hernández, A. J. Miller, J. R. Spence, A. Nusrat, et al., *Nat. Cell Biol. 2017 1911* **2017** , *19* , 1326.

[13] T. Y. Lin, C. S. Ki, C. C. Lin, *Biomaterials***2014** , *35* , 6898.

[14] K. Takayama, K. Kawabata, Y. Nagamoto, K. Kishimoto, K. Tashiro, F. Sakurai, M. Tachibana, K. Kanda, T. Hayakawa, M. K. Furue, et al., *Biomaterials* **2013** , *34* , 1781.

[15] M. J. Powers, K. Domansky, M. R. Kaazempur-Mofrad, A. Kalezi, A. Capitano, A. Upadhyaya, P. Kurzawski, K. E. Wack, D. B. Stolz, R. Kamm, et al., *Biotechnol. Bioeng.* **2002** , *78* , 257.

[16] M. Mansouri, S. Beemer, C. R. Kothapalli, T. Rhoades, P. S. Fodor, D. Das, N. D. Leipzig, *ACS Appl. Mater. Interfaces***2022** , acsami.1c19962.

[17] A. E. Wilkinson, L. J. Kobelt, N. D. Leipzig, *J. Biomed. Mater. Res. Part A* **2013** , *102* , n/a.

[18] J. G. Riess, *Artif. Cells. Blood Substit. Immobil. Biotechnol.* **2005** , *33* , 47.

[19] J. Jägers, A. Wrobeln, K. B. Ferenz, *Pflugers Arch. Eur. J. Physiol.* **2021** , *473* , 139.

[20] T. C. Sunarti, M. I. Febrian, E. Ruriani, I. Yuliasih,*Int. J. Biomater.* **2019** , *2019* .

[21] M. Timur, A. Paşa, *ACS Omega* **2018** , *3* , 17416.

[22] Y. Wang, A. Liu, *Chem. Soc. Rev.* **2020** ,*49* , 4906.

[23] A. Wijekoon, N. Fountas-Davis, N. D. Leipzig, *Acta Biomater.* **2013** , *9* , 5653.

[24] H. Li, A. Wijekoon, N. D. Leipzig, *Ann. Biomed. Eng.***2014** , *42* , 1456.

[25] Z. Jiang, X. Yu, S. Zhai, Y. Hao, *Sensors (Basel).***2017** , *17* , E548.

[26] S. Akula, I. K. Brosch, N. D. Leipzig, *Ann. Biomed. Eng.***2017** , *45* , 2693.

[27] P. PS, F.-D. N, H. H, M. E.-C. M, F. JA, S. LP, L. ND,*Acta Biomater.* **2016** , *36* , 164.

[28] E. Lambert, J. M. Janjic, *Sci. Reports 2021 111***2021** , *11* , 1.

[29] M. Hashem, M. Weiler-Sagie, P. Kuppusamy, G. Neufeld, M. Neeman, A. Blank, *J. Magn. Reson.* **2015** , *256* , 77.

[30] H. M. Tse, G. Gardner, J. Dominguez-Bendala, C. A. Fraker,*Front. Bioeng. Biotechnol.* **2021** , *9* , 241.

[31] I. Godet, S. Doctorman, F. Wu, D. M. Gilkes, *Cells***2022** , *11* .

[32] H. C. Gerritsen, R. Sanders, A. Draaijer, C. Ince, Y. K. Levine, *J. Fluoresc. 1997 71* **1997** , *7* , 11.

[33] S. Breitkopf, T. Eidam, A. Klenke, L. Von Grafenstein, H. Carstens, S. Holzberger, E. Fill, T. Schreiber, F. Krausz, A. Tünnermann, et al., *Light Sci. Appl. 2014 310* **2014** ,*3* , e209.

[34] C. A. Custódio, C. M. Alves, R. L. Reis, J. F. Mano, *J. Tissue Eng. Regen. Med.* **2010** , *4* , 316.

[35] F. Y. Chen, J. J. Yan, H. X. Yi, F. Q. Hu, Y. Z. Du, H. Yuan, J. You, M. D. Zhao, *Int. J. Nanomedicine* **2014** , *9* , 4597.

[36] M. H. Ho, D. M. Wang, H. J. Hsieh, H. C. Liu, T. Y. Hsien, J. Y. Lai, L. T. Hou, *Biomaterials* **2005** , *26* , 3197.

[37] D. L. Taylor, J. J. Thevarajah, D. K. Narayan, P. Murphy, M. M. Mangala, S. Lim, R. Wuhrer, C. Lefay, M. D. O'Connor, M. Gaborieau, et al., *Anal. Bioanal. Chem.* **2015** , *407* , 2543.

[38] J. W. Kuo, D. A. Swarm, G. D. Prestwich, *Bioconjug. Chem.* **1991** , *2* , 232.

[39] I. Pilipenko, V. Korzhikov-Vlakh, V. Sharoyko, N. Zhang, M. Schäfer-Korting, E. Rühl, C. Zoschke, T. Tennikova, *Pharmaceutics***2019** , *11* .

[40] O. Germershaus, S. Mao, J. Sitterberg, U. Bakowsky, T. Kissel,*J. Control. Release* **2008** , *125* , 145.

[41] M. D. Buschmann, A. Merzouki, M. Lavertu, M. Thibault, M. Jean, V. Darras, *Adv. Drug Deliv. Rev.* **2013** , *65* , 1234.

[42] Y. C. Huang, C. C. Huang, Y. Y. Huang, K. S. Chen, *J. Biomed. Mater. Res. - Part A* **2007** , *82* , 842.

[43] L. K. Kanninen, R. Harjumäki, P. Peltoniemi, M. S. Bogacheva, T. Salmi, P. Porola, J. Niklander, T. Smutný, A. Urtti, M. L. Yliperttula, et al., *Biomaterials* **2016** , *103* , 86.

[44] K. Cameron, R. Tan, W. Schmidt-Heck, G. Campos, M. J. Lyall, Y. Wang, B. Lucendo-Villarin, D. Szkolnicka, N. Bates, S. J. Kimber, et al., *Stem Cell Reports* **2015** , *5* , 1250.

[45] C. M. Horejs, A. Serio, A. Purvis, A. J. Gormley, S. Bertazzo, A. Poliniewicz, A. J. Wang, P. DiMaggio, E. Hohenester, M. M. Stevens,*Proc. Natl. Acad. Sci. U. S. A.* **2014** , *111* , 5908.

[46] M. Klaas, K. Möll, K. Mäemets-Allas, M. Loog, M. Järvekülg, V. Jaks, *Sci. Rep.* **2021** , *11* , 1.

[47] X. Peng, L. E. Cuff, C. D. Lawton, K. A. DeMali, *J. Cell Sci.* **2010** , *123* , 567.

[48] Y. Kikkawa, R. Sudo, J. Kon, T. Mizuguchi, M. Nomizu, K. Hirata, T. Mitaka, *Exp. Cell Res.* **2008** , *314* , 2579.

[49] R. Nishiuchi, J. Takagi, M. Hayashi, H. Ido, Y. Yagi, N. Sanzen, T. Tsuji, M. Yamada, K. Sekiguchi, *Matrix Biol.***2006** , *25* , 189.

[50] J. Cho, D. F. Mosher, *J. Thromb. Haemost.* **2006** ,*4* , 943.

[51] Y. Takada, X. Ye, S. Simon, *Genome Biol.* **2007** ,*8* , 215.

[52] N. Kawakami-Kimura1, T. Narita1, K. Ohmori2, T. Yoneda2, K. Matsumoto3, T. Nakamura3, R. Kannagi1l4, *Br. Joumal Cancer***1997** , *75* , 47.

[53] S. Y. Lee, D. Kim, S. H. Lee, J. H. Sung, *APL Bioeng.***2021** , *5* , 041505.

[54] G. Benton, E. Crooke, J. George, *FASEB J.* **2009** ,*23* , 3884.

[55] T. A. Brieva, P. V. Moghe, *Biotechnol. Bioeng.***2001** , *76* , 295.

[56] K. Wake, *Proc. Japan Acad. Ser. B Phys. Biol. Sci.***2006** , *82* , 155.

[57] A. Akhavan, O. L. Griffith, L. Soroceanu, D. Leonoudakis, M. G. Luciani-Torres, A. Daemen, J. W. Gray, J. L. Muschler, *Cancer Res.* **2012** , *72* , 2578.

[58] H. Urushima, H. Yuasa, T. Matsubara, N. Kuroda, Y. Hara, K. Inoue, K. Wake, T. Sato, S. L. Friedman, K. Ikeda, *Am. J. Pathol.***2021** , *191* , 438.

[59] E. A. Cavalcanti-Adam, T. Volberg, A. Micoulet, H. Kessler, B. Geiger, J. P. Spatz, *Biophys. J.* **2007** , *92* , 2964.

[60] S. Singla, K. Z. Htut, R. Zhu, A. Davis, J. Ma, Q. Z. Ni, M. D. Burkart, C. Maurer, T. Miyoshi, A. Dhinojwala, *ACS Omega***2021** , *6* , 35514.